A VAD-Based Dealiasing Method for Radar Velocity Data Quality Control

QIN XU

NOAA/National Severe Storms Laboratory, Norman, Oklahoma

KANG NAI, LI WEI, AND PENGFEI ZHANG

Cooperative Institute for Mesoscale Meteorological Studies, University of Oklahoma, Norman, Oklahoma

SHUN LIU

I. M. Systems Group Inc., Camp Springs, Maryland

DAVID PARRISH

NOAA/National Centers of Environmental Prediction, Camp Springs, Maryland

(Manuscript received 19 January 2010, in final form 23 August 2010)

ABSTRACT

This paper describes a new velocity–azimuth display (VAD)-based dealiasing method developed for automated radar radial velocity data quality control to satisfy the high-quality standard and efficiency required by operational radar data assimilation. The method is built on an alias-robust velocity–azimuth display (AR-VAD) analysis. It upgrades and simplifies the previous three-step dealiasing method in three major aspects. First, the AR-VAD is used with sufficiently stringent threshold conditions in place of the original modified VAD for the preliminary reference check to produce alias-free seed data in the first step. Second, the AR-VAD is more accurate than the traditional VAD for the refined reference check in the original second step, so the original second step becomes unnecessary and is removed. Third, a block-to-point continuity check procedure is developed, in place of the point-to-point continuity check in the original third step, which serves to enhance the use of the available seed data in a properly enlarged block area around each flagged data point that is being checked with multiple threshold conditions to avoid false dealiasing. The new method has been tested extensively with aliased radial velocity data collected under various weather conditions, including hurricane high-wind conditions. The robustness of the new method is exemplified by the results tested with three cases. The limitations of the new method and possible improvements are discussed.

1. Introduction

It is well known in radar meteorology that there is a maximum velocity, called the Nyquist velocity v_N, beyond which the measured radial velocities are aliased back into the Nyquist interval between $\pm v_N$ (Doviak and Zrnić 2006, section 3.6). Radar radial velocity aliasing usually can be detected from abrupt velocity changes of about $2v_N$ between neighboring measurements, but correcting aliased velocities is nontrivial and often requires additional independent wind information to provide some reference points (Ray and Ziegler 1977; Hennington 1981; Bergen and Brown 1980; Bergen and Albers 1988). Because aliasing can occur in countless different ways and the aliasing scenarios can be extremely complex, considerable efforts have been made in developing various techniques to correct aliased velocities (Eilts and Smith 1990; Jing and Wiener 1993; Yamada and Chong 1999; James and Houze 2001; Tabary et al. 2001; Gong et al. 2003; Haase and Landelius 2004; Gao et al. 2004; Zhang and Wang 2006; Zhu and Gong 2006). The techniques developed thus far, however, are still not sufficiently robust to deal with every severely aliased situation and correct or flag all aliased radar radial velocities. On the radar engineering side, the staggered pulse repetition time (PRT) technique (Torres et al. 2004; also see Doviak and Zrnić 2006, section 7.4.3) can be implemented to

Corresponding author address: Dr. Qin Xu, 120 David L. Boren Blvd., National Severe Storms Laboratory, Norman, OK 73072-7326.
E-mail: qin.xu@noaa.gov

DOI: 10.1175/2010JTECHA1444.1

Report Documentation Page

Form Approved
OMB No. 0704-0188

1. REPORT DATE	2. REPORT TYPE	3. DATES COVERED
AUG 2010		**00-00-2010 to 00-00-2010**

4. TITLE AND SUBTITLE
A VAD-Based Dealiasing Method for Radar Velocity Data Quality Control

5a. CONTRACT NUMBER
5b. GRANT NUMBER
5c. PROGRAM ELEMENT NUMBER

6. AUTHOR(S)

5d. PROJECT NUMBER
5e. TASK NUMBER
5f. WORK UNIT NUMBER

7. PERFORMING ORGANIZATION NAME(S) AND ADDRESS(ES)
NOAA/National Severe Storms Laboratory,120 David L. Boren Blvd,Norman,OK,73072-7326

8. PERFORMING ORGANIZATION REPORT NUMBER

9. SPONSORING/MONITORING AGENCY NAME(S) AND ADDRESS(ES)

10. SPONSOR/MONITOR'S ACRONYM(S)
11. SPONSOR/MONITOR'S REPORT NUMBER(S)

12. DISTRIBUTION/AVAILABILITY STATEMENT
Approved for public release; distribution unlimited

13. SUPPLEMENTARY NOTES

14. ABSTRACT

This paper describes a new velocity?azimuth display (VAD)-based dealiasing method developed for automated radar radial velocity data quality control to satisfy the high-quality standard and efficiency required by operational radar data assimilation. The method is built on an alias-robust velocity?azimuth display (AR-VAD) analysis. It upgrades and simplifies the previous three-step dealiasing method in three major aspects. First, the AR-VAD is used with sufficiently stringent threshold conditions in place of the original modifiedVADfor the preliminary reference check to produce alias-free seed data in the first step. Second, the AR-VAD is more accurate than the traditional VAD for the refined reference check in the original second step, so the original second step becomes unnecessary and is removed. Third, a block-to-point continuity check procedure is developed, in place of the point-to-point continuity check in the original third step, which serves to enhance the use of the available seed data in a properly enlarged block area around each flagged data point that is being checked with multiple threshold conditions to avoid false dealiasing. The new method has been tested extensively with aliased radial velocity data collected under various weather conditions, including hurricane high-wind conditions. The robustness of the new method is exemplified by the results tested with three cases. The limitations of the new method and possible improvements are discussed.

15. SUBJECT TERMS

16. SECURITY CLASSIFICATION OF:			17. LIMITATION OF ABSTRACT	18. NUMBER OF PAGES	19a. NAME OF RESPONSIBLE PERSON
a. REPORT	b. ABSTRACT	c. THIS PAGE			
unclassified	**unclassified**	**unclassified**	**Same as Report (SAR)**	**13**	

mitigate the velocity aliasing problem and extend the unambiguous range. At the lowest few elevations, however, a uniform PRT is required for effective ground clutter filtering. For this reason, and to mitigate the range folding, the phase-coding technique (Frush et al. 2002) has been recently implemented on the uniform PRT. Because of this, radar velocity aliasing will remain a serious problem for low-elevation scans (because of the use of uniform PRT).

Radar data quality control is critical for radar data assimilation, and dealiasing is an important and yet often very difficult part of radar data quality control. The dealiasing technique (Eilts and Smith 1990) used on Weather Surveillance Radar-1988 Doppler (WSR-88D) radars [the Next Generation Weather Radar (NEXRAD) network] for processing real-time radar data was developed primarily for visual and certain quantitative applications, with considerable tolerance for bad or poor quality data, to retain the original data coverage as much as possible. Therefore, the processed data often do not satisfy the high-quality standard required by data assimilation at the National Centers of Environmental Prediction (NCEP). This problem is common for most dealiasing techniques developed thus far, especially for those designed primarily for visual applications. Striving to meet the need of radar data assimilation, Gong et al. (2003) developed a three-step dealiasing method. In this method, the modified velocity–azimuth display (VAD) technique (Mod-VAD) of Tabary et al. (2001) was adopted and applied to raw (aliased) velocity data to estimate horizontal vector velocities averaged on selected range circles of radar scans. These velocities were used as preliminary references for pre-dealiasing. Then, the traditional VAD analysis (Lhermitte and Atlas 1961; Browning and Wexler 1968) was applied to the pre-dealiased velocity data to produce refined reference radial velocities for dealiasing in the second step. After these two steps, the dealiased velocities along the boundary of each flagged area were used as starting points for the point-to-point continuity check in the third step.

The above Mod-VAD-based three-step dealiasing method was successfully tested with many cases of aliased radar radial velocity observations, including difficult cases of severely aliased radial velocity observations collected during tornadic storms. The method was later included in a package for radar radial velocity quality control (Zhang et al. 2005; Liu et al. 2005a, 2009) and delivered to NCEP for operational tests to satisfy the radar data assimilation need. During the operational tests, some particularly difficult cases were encountered in which the three-step method failed to detect or correct severely aliased radial velocities. Having diagnosed the failures in detail, the following two reasons have been identified. (i) The Mod-VAD adopted in the first step is not sufficiently robust to deal with severely aliased radial velocities [because of the weaknesses explained in the introduction of Xu et al. (2010)], and the dealiasing threshold condition used in this step is not sufficiently stringent to avoid false dealiasing, especially when the Mod-VAD fails to perform well at too many vertical levels to yield a reliable vertical profile of VAD wind. In many cases, the Mod-VAD failed badly or even completely, and some of the failures were reported in Xu et al. (2010, see the last paragraphs of sections 3.3, 4.2 and 4.3 therein). (ii) The point-to-point continuity check in the third step requires seed data in the neighborhood area of each flagged data point that is being checked, so it cannot pass an area that has no seed datum within five gates along the previous and current beams from the flagged data point. Here, by definition, seed data are those that pass all of the threshold conditions in the previous step. Additionally, the dealiasing threshold condition used by the point-to-point continuity check is also not sufficiently stringent, so a falsely dealiased radial velocity can occasionally pass the threshold condition to yield a false seed datum, and thus can cause continued false dealiasing in subsequently checked areas.

To eliminate the above sources of false dealiasing, the recently developed alias-robust VAD technique (AR-VAD; Xu et al. 2010) is used in this paper to replace the Mod-VAD for the preliminary reference check in the first step. After this, the traditional VAD analysis and refined reference check in the second step become unnecessary, and thus can be bypassed. In addition, a block-to-point continuity check is designed to replace the point-to-point continuity check in the third step of the previous three-step dealiasing method. With these major upgrades, the performance and robustness of the method are greatly improved. The new method is described in the next section. Three examples are presented in section 3 to show the robustness of the new method. The limitations of this new AR-VAD-based method and possible improvements are discussed with the conclusions in section 4.

2. Description of the method

a. Data preprocessing

When the AR-VAD (Xu et al. 2010) is used to estimate the vertical profile of the horizontal vector wind, denoted by (u_0, v_0), averaged over the horizontal area covered by the radar radial velocity observations, the VAD wind direction is derived from the two zero points of $v_r(\phi)$ that are searched and estimated on each qualified vertical level [see section 4.3 of Xu et al. (2010) for the qualification criteria], where $v_r(\phi)$ denotes the true radial velocity as a function of the azimuthal angle ϕ (clockwise with respect to the y coordinate pointing to the north). In the presence of aliasing, the observed

radial velocities can become nearly zero over a small azimuthal range, which often contains an aliased zero point. The absolute value of the azimuthal derivative estimated at such an aliased zero point should be smaller than that estimated at the true zero point (where the azimuthal derivative has the same sign as that at the aliased zero point), and this criterion can be used to distinguish the two true zero points from aliased zero points (see appendix A of Xu et al. 2010). Occasionally, however, observed radial velocities can be contaminated (by ground clutter, especially in the presence of anomalous propagation, though for reasons not completely clear) to become falsely near zero (<1.5 m s^{-1}) over an azimuthally extended sector ($>20°$), and thereby interfere in the search for the true zero points. Thus, before the first step starts, the data need to be preprocessed to not only remove isolated data points (as in Gong et al. 2003) but also flag large sector areas where the observed radial velocities are near zero. The preprocessing contains the following four substeps:

1) Check and remove isolated observations over each tilt by the following two sweeping procedures. In the first procedure, an observation is considered to be an isolated one and thus removed if there are no more than three other observations available in the $3\Delta r \times 3°$ box area centered on this observation point, where Δr ($=250$ m) is the range gate spacing. In the second procedure, an observation is considered to be an isolated one and is removed if there is no other observation in the $3\Delta r \times 3°$ box area centered on this observation point. This step was adopted from Bergen and Albers (1988) and used in the previous three-step method (Gong et al. 2003).
2) Check and remove isolated data pairs (which are most likely contaminated by flying objects, such as airplanes) along each circle of fixed range distance from the radar. Such a circle will be called the ''range circle'' (or simply ''circle'' hereafter). After all of the isolated observations are removed in the above substep 1, an observation must belong to an isolated pair, and this pair should be removed if there is only one other observation in the $\pm 2°$ vicinity of this observation point along the circle. This substep is new.
3) Check and remove nearly empty range circles that are most likely contaminated by the range folding. A range circle is considered to be nearly empty if it contains no more than four observations. This substep is also new. Substeps 1, 2, and 3 apply to all data, and their rejected data will not be used in any subsequent steps.
4) Check each $5\Delta r \times 21°$ box area (centered on each observation point) over each tilt, and flag all of the observations in the box area if more than 75% of the observations in the box are smaller than 1.5 m s^{-1}. Then, check each circle and flag all of the observations in the circle if more than 10 continuously distributed observations are smaller than 0.5 m s^{-1} or more than 20 observations are smaller than 0.5 m s^{-1}. This substep is new and is designed to flag near-zero radial velocity sectors for the reason explained above.

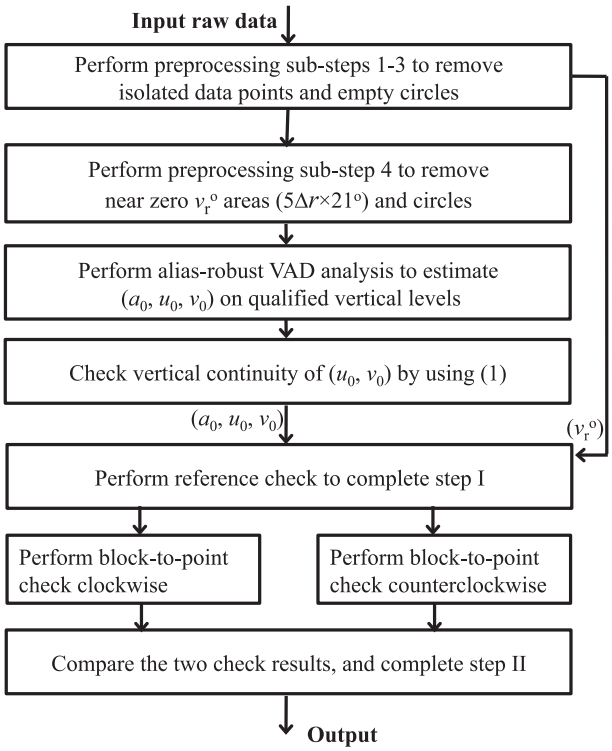

FIG. 1. Main flowchart for the new VAD-based method.

The above four substeps are shown by the first two boxes in the main flowchart plotted in Fig. 1. Note that the flagged observations by substep 4 will not be used to estimate the VAD parameters but will be used together with all of the nonflagged as input radial velocity data for the reference check after the VAD parameters are estimated. Thus, the raw data must pass all of the above four substeps before they can be used by AR-VAD analysis to estimate the three VAD parameters for the subsequent reference check, and this is indicated by the arrow labeled with (a_0, u_0, v_0) from the fourth to the fifth box in Fig. 1. However, the input radial velocity observations (denoted by v_r^o) for the reference check only need to pass the above substeps 1–3; this is shown by the long bypassing arrow labeled with (v_r^o) on the right-hand side of Fig. 1.

b. First step: Reference check based on alias-robust VAD analysis

In this step, the AR-VAD is used to estimate the vertical profile of the parameters averaged over the

horizontal area covered by the radar radial velocity observations. The parameters estimated by the AR-VAD from a selected range circle include not only the averaged horizontal vector wind (u_0, v_0) in the first-order harmonic term but also the entire zeroth-order harmonic term, parameterized by a_0, in the truncated Fourier expansion of the VAD-parameterized radial velocity [see Eq. (2)]. As described in appendix B of Xu et al. (2010), these three parameters are estimated at each qualified vertical level by using all of the observations from the qualified and semiqualified range circles on different tilts. The vertical level (beam height) is computed by considering the effects of the standard atmospheric refraction and the earth's curvature [see (2.28b) of Doviak and Zrnić 2006]. The searching procedure for qualified vertical levels starts from $z = 250$ m above the radar site and goes up with an increment of $\Delta z = 50$ m. The starting level of $z = 250$ m is selected empirically to avoid possible ground clutter contamination. The vertical increment of $\Delta z = 50$ m is the same as that used by the Mod-VAD for the reference check in the previous three-step method (Gong et al. 2003) and is found to be still adequate and efficient for the AR-VAD-based reference check in this paper. Based on our additional tests (not shown), reducing Δz (to 25 m) does not yield any significant improvement or change for the reference check, but it does reduce the computational efficiency.

To avoid possible contamination caused by ground clutter residuals, no qualified or semiqualified range circle should be selected from the lowest tilt ($\theta \approx 0.5°$), even if the radar volumetric scan contains a very limited number of tilts [such as the operational scan mode volume coverage pattern (VCP)32 that has only five tilts at 0.5°, 1.5°, 2.5°, 3.5°, and 4.5° for clear weather]. Excluding the lowest tilt may not be sufficient by itself to avoid contamination caused by ground clutter residuals (especially in the presence of terrain and anomalous propagation). However, because near-zero radial velocity areas (including those caused by ground clutter in the presence of terrain and anomalous propagation) have been largely removed by the preprocessing (see section 2a), we have not seen any significant problem by excluding only the lowest tilt (for VCP32) from the tests performed thus far (see the first paragraph of section 3). Nevertheless, if the radar volumetric scan contains a large number of tilts (such as the scan mode VCP11 or VCP12, with 14 tilts from 0.5° to 19.5° for convective precipitation, or scan mode VCP21, with nine tilts from 0.5° to 19.5° for stratiform precipitation), then it will be safe to not select either a qualified or semiqualified range circle from the tilts below 4.0°. This enhanced restriction (for VCP11, VCP12, and VCP21) is new and was not reported in appendix B of Xu et al. (2010) for the AR-VAD. Additionally, the following two additional restrictions are imposed to avoid large gaps and large jumps in the estimated vertical profile of (u_0, v_0):

(i) The searching procedure will stop and will not restart at a higher level [see the end of step III in appendix B of Xu et al. (2010)] if no qualified vertical level is found within 2 km above the previous qualified vertical level.

(ii) If a qualified vertical level is found within 2 km above the previous qualified vertical level, then the estimated (u_0, v_0) at this vertical level is acceptable only if its difference, denoted by (Δu_0, Δv_0), from that estimated at the previous qualified vertical level satisfies

$$\max(|\Delta u_0|, |\Delta v_0|) < 6\,\mathrm{m\,s^{-1}}. \quad (1)$$

If the threshold condition in (1) is not satisfied, then the searching procedure will also stop and will not get to the next higher level.

The threshold condition in (1) is independent of the gap between the two qualified vertical levels, but the gap can neither be smaller than 50 m nor larger than 2 km. By restricting the change of (u_0, v_0) over each vertical gap, this threshold condition avoids inaccurate or unreliable reference radial velocities computed by interpolating (u_0, v_0) to the observation points within the gap (between the two adjacent qualified vertical levels). The threshold value (6 m s^{-1}) in (1) is set empirically and conservatively. This setting has passed all of the tests performed thus far (see the first paragraph of section 3), although the selected value or even the form of (1) could be fine-tuned for each type of scenario or application. It may occasionally reject valid estimates of (u_0, v_0) in a layer of strong vertical shear, but this is the price paid for safeguarding to avoid any unreal large jumps in the estimated vertical profile of (u_0, v_0). The AR-VAD analysis and vertical continuity check are shown by the third and fourth boxes, respectively, in the main flowchart plotted for the new method in Fig. 1.

To search for qualified vertical levels, the procedure starts from the lowest vertical level (at $z = 250$ m above the radar site) and goes upward every $\Delta z = 50$ m until no qualified vertical level can be found within 2 km above the previous qualified vertical level. The procedure does not restart beyond 2 km above the previous qualified vertical level, and this modifies the procedure in appendix B of Xu et al. (2010). Therefore, the VAD parameters (a_0, u_0, and v_0) estimated at the qualified vertical levels are ensured to have no vertical gap larger than 2 km. As explained earlier, this upper limit for the vertical gap is prerequired by the threshold condition in (1).

Because the estimated VAD parameters are not interpolated across a vertical gap larger than 2 km, they may sometimes cover only a small vertical range, and their produced reference radial velocities may cover a very limited radial range, especially as θ becomes large. In this case, according to our extensive tests, the reference check in the first step still can provide enough seed data for the block-to-point check in the second step.

Once the VAD parameters (a_0, u_0, v_0) estimated at the qualified vertical levels are interpolated to the vertical level of a selected range circle on a given tilt, the reference radial velocity is computed at each observation point on the selected range circle by the following relationship [see (2) of Xu et al. 2010]:

$$v_r^{\text{ref1}} = a_0 + \cos\theta(u_0 \sin\phi + v_0 \cos\varphi), \tag{2}$$

where $(\ )_0$ denotes the averaged value of $(\ )$ over the horizontal area covered by the radar radial velocity observations, $a = (w - w_T)\sin\theta + r\cos^2\theta(\partial u/\partial x + \partial v/\partial y)/2$, θ is the elevation angle, r is the radial range of the circle, w is the air motion vertical velocity, w_T is the downward hydrometeor's terminal fall velocity, and $\partial u/\partial x + \partial v/\partial y$ is the divergence of the horizontal wind. Strictly speaking, in (2) θ should be the slope angle of the beam relative to the earth's surface beneath the measurement point that deviates gradually away from the elevation angle as r increases from zero resulting from the atmospheric refraction and the earth's curvature [see (9.9) of Doviak and Zrnić 2006]. However, because (2) is also used by the AR-VAD to estimate a_0 and (u_0, v_0), the reference radial velocity v_r^{ref1} computed by (2) from the estimated a_0 and (u_0, v_0) is along the same beam, and thus must be exactly at the same beam height as the observed radial velocity v_r^o that is being checked. It is thus unnecessary to know the beam height for the reference check. In this sense, the reference check is not affected by the atmospheric refraction and the earth's curvature.

The computed v_r is used for the reference check. The check goes through each data point along each circle, from the smallest circle on each tilt until it reaches the largest radial range (corresponding to the top vertical level attained by the VAD analysis) or the cut-off radial range ($r = 30$ km if $\theta \approx 0.5°$, or $r = 80$ km if $\theta \geq 1°$), whichever is reached first. The cut-off radial ranges are new for the reference check in this paper, and they are imposed to avoid possible false dealiasing (caused by the deteriorated validity of the VAD uniform-wind assumption at an increasingly far radial range in a scenario of strongly nonuniform wind). Their values are tuned and selected based on our extensive tests of the new method (see the first paragraph of section 3). In addition, the alias correction threshold used by the reference check here is more stringent than used by the reference check in the three-step method (Gong et al. 2003). In particular, the Nyquist folding number is estimated by

$$N = \text{Int}[(v_r^{\text{ref1}} - v_r^o)/2v_N], \tag{3}$$

where $\text{Int}[(\ )/2v_N]$ represents the nearest integer of $(\ )/2v_N$, v_r^o is the observed radial velocity, and v_N is the Nyquist velocity. If $N = 0$, then the observed radial velocity needs no correction, but it is accepted as a seed datum only if it satisfies

$$|v_r^o - v_r^{\text{ref1}}| \leq v_N/4. \tag{4}$$

If $N \neq 0$, then the radial velocity is corrected from v_r^o to v_r^{o1} $(= v_r^o + 2Nv_N)$, but the correction is accepted as a new seed datum (in place of the original v_r^o) only if it satisfies

$$|v_r^{o1} - v_r^{\text{ref1}}| \leq v_N/4. \tag{5}$$

The threshold value of $v_N/4$ used in (4) and (5) is smaller and thus more stringent than the commonly used threshold value of $v_N/2$ (Hennington 1981; James and Houze 2001; Gong et al. 2003). If neither (4) nor (5) are satisfied, then the data point is flagged and the check proceeds to the next data point. The accepted observations and corrections by the reference check within the cut-off radial ranges (30 km for $\theta \approx 0.5°$ and 80 km for $\theta \geq 1°$) will be used as seed data for the block-to-point continuity check in the next step.

In the previous three-step dealiasing method, the Mod-VAD was adopted to estimate the horizontal vector wind (u_0, v_0), but it could not estimate a_0, so v_r^{ref1} was computed approximately by setting $a_0 = 0$ in (2) for the preliminary reference check in the first step. After this step, the traditional VAD analysis was applied to the dealiased data to estimate (u_0, v_0) together with a_0. These three estimated parameters were then used for the refined reference check in the second step. As explained in Gong et al. (2003), the quality of the refined reference check depended critically on the accuracy of the estimated (u_0, v_0) and a_0, while the latter depended critically on the quality of the dealiased data obtained by the preliminary reference check by using v_r^{ref1} computed approximately from the crudely estimated (u_0, v_0) by the Mod-VAD. Because of this, the dealiased data on each selected circle in the first step were further checked and reselected through additional quality controls and then used to produce traditional VAD analysis

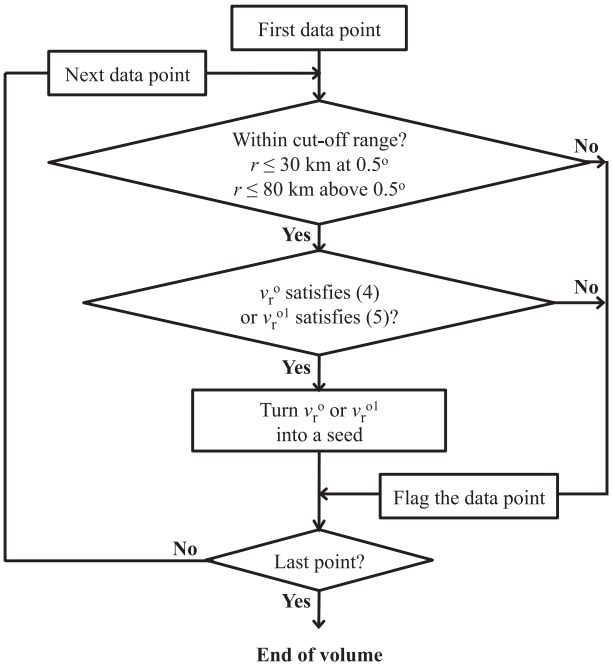

FIG. 2. Flowchart for the reference check in the first step.

for the refined reference check in the second step (see Gong et al. 2003, section 2c). The AR-VAD estimates (u_0, v_0) together with a_0 directly, and the analysis is more accurate than not only the Mod-VAD analysis in the first step, but also the traditional VAD analysis in the second step of the previous three-step method. When the AR-VAD is used in place of the Mod-VAD in the first step, the refined reference check in the original second step becomes redundant and is thus removed from the new method. The flowchart for the reference check in the first step is shown in Fig. 2, while the reference check is performed through the third box from the bottom of the main flowchart in Fig. 1.

c. *Second step: Block-to-point continuity check*

In this second step, a block-to-point continuity check is used to replace the point-to-point continuity check in the original third step of the three-step dealiasing method. The check performs two procedures—clockwise and counterclockwise—in parallel on each tilt. The clockwise (counterclockwise) procedure goes clockwise (counterclockwise) along each circle (starting from $\phi = 0$) and processed circle-by-circle from the smallest circle to the largest circle on each tilt. The procedure searches for flagged data points clockwise (counterclockwise) along each circle. No action is taken at a nonflagged data point. Once a flagged point is found, this point is checked through the following two substeps:

1) Search for seed data backward toward the radar up to 40 gates (10 km, not including the current gate) along each of the 11 beams in the ±5° vicinity of the current flagged data point. If there are no more than 40 seed data, then the flag remains and the process goes to the next flagged data point. If there are 40 or more seed data, then compute the mean radial velocity from the searched seed data and use it as the reference, denoted by v_r^{ref2}, to check the flagged radial velocity v_r^o. If the flagged radial velocity v_r^o satisfies

$$|v_r^o - v_r^{\text{ref2}}| \le v_N/2, \tag{6}$$

then the flagged data point is turned into a seed data point and the process goes to the next flagged data point. Otherwise, compute the Nyquist folding number by using (3) with v_r^{ref1} replaced by v_r^{ref2}, and then correct the flagged radial velocity from v_r^o to v_r^{o2} $(=v_r^o + 2Nv_N)$. If the correction v_r^{o2} does not satisfy following threshold condition:

$$|v_r^{o2} - v_r^{\text{ref2}}| \le v_N/2, \tag{7}$$

then the flag remains and the process goes to the next flagged data point. If the correction v_r^{o2} satisfies (7), then it needs additional checks in next substep.

2) Perform the following three additional checks of v_r^{o2} in parallel:
   (i) Search for the first seed datum along the current beam backward toward the radar up to 10 gates from the current gate. If such a seed datum is found, denoted by v_r^{seed1}, and v_r^{o2} satisfies

$$|v_r^{o2} - v_r^{\text{seed1}}| \le \max(v_N/3, 6\,\text{m s}^{-1}), \tag{8}$$

   then this first check is passed. Otherwise, the check fails.
   (ii) Search for the first seed datum along the current circle backward counterclockwise (or clockwise) up to 5° from the current azimuth angle. If such a seed datum is found, denoted by v_r^{seed2}, and v_r^{o2} satisfies

$$|v_r^{o2} - v_r^{\text{seed2}}| \le \max(v_N/4, 5\,\text{m s}^{-1}), \tag{9}$$

   then this second check is passed. Otherwise, the check fails.
   (iii) Search for the first seed datum along the previous circle forward clockwise (or counterclockwise) up to 5° from the current azimuth angle. If such a seed datum is found, denoted by v_r^{seed3}, and v_r^{o2} satisfies

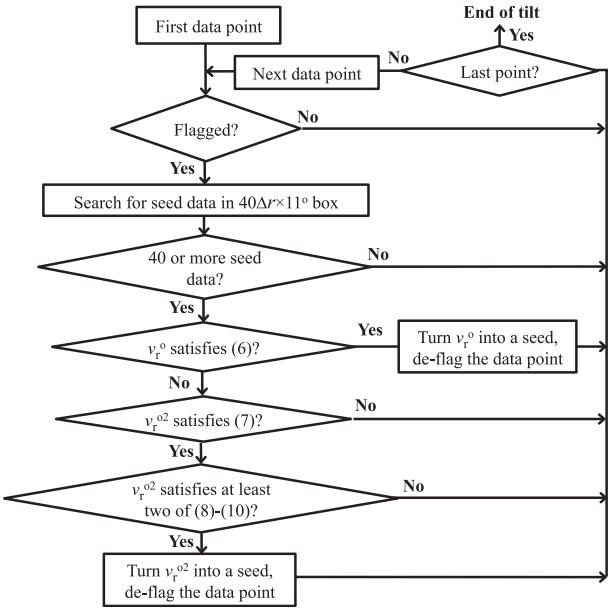

FIG. 3. Flowchart for the clockwise (or counterclockwise) procedure of the block-to-point continuity check in the second step.

$$|v_r^{o2} - v_r^{\text{seed3}}| \le \max(v_N/4, 5\ \text{m s}^{-1}), \quad (10)$$

then this third check is passed. Otherwise, the check fails.

If two or all the above three additional checks are passed, then the corrected radial velocity v_r^{o2} is accepted as a new seed datum (in place of the original v_r^o), and the data point is deflagged at this stage for the clockwise (or counterclockwise) procedure only. Otherwise, the flag remains and the process goes to the next flagged data point.

After the clockwise and counterclockwise procedures go in parallel through the entire tilt, the results from the two procedures are compared to mutually recheck all of the corrections v_r^{o2}. If two identical (or different) corrections are made and accepted by the two procedures at the same data point, then these corrections pass (or fail to pass) the recheck. If only one correction is made and accepted (by one procedure), then this correction passes the recheck (although this data point is flagged by another procedure). As soon as all of the corrections are rechecked, the block-to-point continuity check is done for the current tilt and proceeds to the next higher tilt until it goes through the entire volume. The flowchart for the clockwise (or counterclockwise) procedure of the block-to-point continuity check in the second step is shown in Fig. 3, while the block-to-point continuity check is performed through the last two boxes of the main flowchart in Fig. 1.

3. Applications to radar observations

The new method has been tested successfully with 12 900 volumes of radial velocity observations scanned by six National Oceanic and Atmospheric Administration (NOAA)/National Weather Service (NWS) operational radars [KINX, KLZK, KSGF, KSRX, KTLX, and KVNX; see Fig. 2 of Xu et al. (2007b)] in the central United States during the passage of a severe frontal storm system over the period from 0000 UTC 20 May to 2300 UTC 28 May 2005. The method also has been successfully tested with severely aliased radial velocity data collected under hurricane high-wind conditions. These include data collected by the (i) KAKQ (292 volumes from 1158 UTC 18 September to 1208 UTC 19 September 2003), KMHX (280 volumes from 1157 UTC 18 September to 1206 UTC 19 September 2003), and KRAX (275 volumes from 1159 UTC 18 September to 1207 UTC 19 September 2003) from long-lived Hurricane Isabel that made landfall near Drum Inlet, North Carolina, on 18–19 September 2003; (ii) KLIX (151 volumes from 0003 to 1349 UTC 29 August 2005), KMOB (275 volumes from 0003 to 2351 UTC 29 August 2005), and KEVX (175 volumes from 0002 to 1430 UTC 29 August 2005) from Hurricane Katrina that caused a devastating disaster along the gulf coast and in New Orleans, Louisiana, on 29 August 2005; and (iii) KHGX (300 volumes from 0000 to 2300 UTC 13 September 2008) from Hurricane Ike that passed over Houston, Texas, on 13 September 2008. Three examples are given in the following subsections to show the performance of the new AR-VAD-based method. The first example is a hurricane case. For this case, the performance of the new method will be analyzed in detail in comparison with the previous Mod-VAD-based three-step method. The second example is a squall-line case, and the third example is a cold front case. For these two cases, the performances of the new method will be discussed in comparison with the operational method (Eilts and Smith 1990). The high data quality standard required by radar data assimilation will be discussed in the last subsction.

a. Hurricane case

Figure 4a is the image of raw radial velocities scanned at $\theta = 0.5°$ by the operational KMHX radar at 2015:46 UTC 18 September 2003 from Hurricane Isabel near Drum Inlet. The spatial resolutions of the scans were 250 m in the radial direction and 1° in the azimuthal direction. At this time, the hurricane center (marked by the blue letter "C" in Fig. 4a) was about 120 km to the north (in the direction of $\phi \approx 350°$) of the KHMX radar. Even though the Nyquist velocity was as large as $v_N = 23.19\ \text{m s}^{-1}$, the observed radial velocities were severely

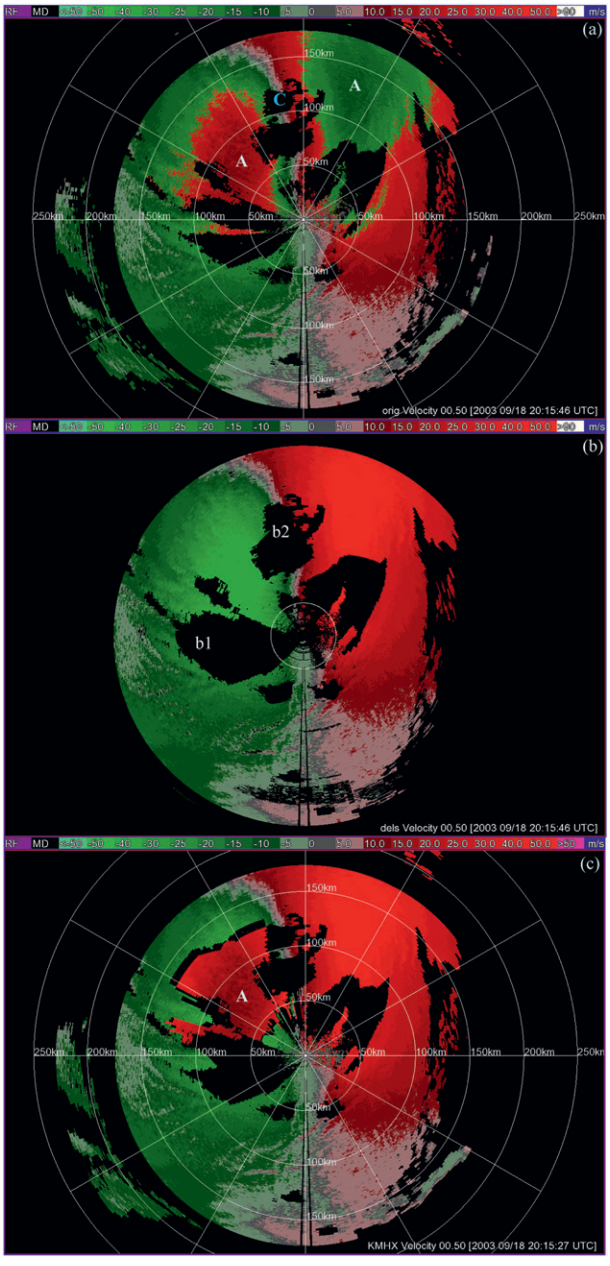

FIG. 4. (a) Raw level-II Doppler radial velocity image on 0.5° elevation from KMHX radar at 2015 UTC 18 Sep 2003. (b) Dealiased radial velocity image by the new AR-VAD-based method. (c) Dealiased radial velocity image by the previous Mod-VAD-based three-step method. (a) The center of Hurricane Isabel is marked by the blue letter C and the main aliased velocity areas are marked by the two white letter "A"s. (b) The white letters b1 and b2 show the flagged (and thus blackened) data areas. (c) The red sector area marked by the white letter A shows false dealiasing.

aliased in the two main areas (marked by the two white "A"s in Fig. 4a)—one is the green area to the east of the hurricane center, and the other is the red area to the southwest of the hurricane center. In addition to the above two main areas, the observed radial velocities were also aliased in the three banded green areas to the east of the radar within 80-km radial range, and in a narrow red area to the west of the radar within 90-km radial range. The above aliased velocities were caused by the intense rotational winds both around and outside of the hurricane eye.

As explained in section 2b, the reference check goes from the smallest radial range only up to $r = 30$ km on the lowest tilt ($\theta = 0.5°$), and the 30-km-range circle is shown by the white circle in Fig. 4b. Within this 30-km-range circle, the aliased radial velocities in the red area to the northwest of the radar and in the green areas to the northeast and east of the radar in Fig. 4a are corrected in Fig. 4b. The corrections are made largely by the reference check in the first step, as revealed by the partially dealiased image produced at the end of the first step (not shown). As shown in Fig. 4a, the raw data are quite noisy and have near-zero values in the immediate vicinity of the radar within the 15-km range, so they are not very reliable and are largely removed (blacked as shown in Fig. 4b) by the preprocessing step (described in section 2a). The dealiased image outside the 30-km-range circle in Fig. 4b is produced by the block-to-point continuity check in the second step. By comparing Fig. 4b with Fig. 4a, it is easy to see that the aliased radial velocities in the two main alias areas (marked by the two white "A"s in Fig. 4a) are corrected by the block-to-point check without any false dealiasing. The aliased radial velocities in the banded green areas to the east of the radar within 80-km radial range in Fig. 4a are also corrected without any false dealiasing.

The corrections made outside the 30-km-range circle in Fig. 4b demonstrate that the block-to-point continuity check can go through (or around) most data holes. The point-to-point continuity check in the previous three-step method (Gong et al. 2003), however, fails to pass through some large data holes, and even occasionally produces false dealiasing. Such a failure is evidenced by the red sector area marked by the white letter A in Fig. 4c. In terms of passing through data holes and avoiding false dealiasing, the block-to-point continuity check performs significantly better and is more robust than the point-to-point continuity check. The improvement comes from the block-averaged reference (v_r^{ref2}) and stringent threshold conditions [see (5)–(9)] used in the design of the block-to-point continuity check, although the design is neither intended nor is it even possible to correct all of the aliased radial velocities and leaves no flagged data points. Similar improvements are seen from the dealiased images (not shown) on all of the remaining tilts above $\theta = 0.5°$.

Because the new dealiasing method is developed as a part of the radar data quality control package for radar

data assimilation applications, avoiding false dealiasing is the most important requirement. To meet this requirement, stringent threshold conditions must be used for alias corrections (see section 2). This will inevitably compromise the alias correction coverage and thus will leave some difficult or ambiguous data that are neither corrected nor deflagged. In particular, the block-to-point continuity check is not able to deflag data points in an isolated data island or nearly isolated data peninsula (stretched toward the radar) surrounded by extensive data-void areas. In addition, the block-to-point continuity check goes only one way—outward away from the radar—in the radial direction, and it searches for seed data only backward from the current circle toward the radar up to 10 km (see section 2c). Because of this, the block-to-point continuity check could not find enough seed data along the narrow strip data peninsular from $r \approx 35$ to 110 km to the west of the radar (see Fig. 4a). This explains why the data points on this narrow strip remain flagged, and thus blackened in Fig. 4b. This narrow strip contains both aliased radial velocities (in the narrow red area to the west of the radar within 90-km radial range in Fig. 4a) and nonaliased radial velocities (in the extended green area over the radial range from 80 to 110 km to the west of the radar in Fig. 4a). The location of this narrow strip is marked as ''b1'' in Fig. 4b. Another flagged and blackened data area is the nearly disconnected segment of the hurricane eyewall image along the southern rim of the hurricane eye in Fig. 4a; this area is marked by ''b2'' in Fig. 4b.

For the hurricane case exemplified above, the alias correction coverage can be further improved by relaxing the cut-off radial range for the reference check in the first step. In particular, if the cut-off radial range is extended from 30 to 50 km, then the flagged data points in the blackened area marked b1 in Fig. 4b can be correctly deflagged up to $r = 50$ km by the reference check in the first step, and then to the full radial range of the narrow strip data peninsula by the block-to-point continuity check in the second step without causing any false dealiasing (not shown). Although relaxing the cut-off radial range for the reference check can improve the alias correction coverage in this and many other cases, it can also occasionally cause false dealiasing. To avoid false dealiasing, it is necessary to impose a short (30 km) cut-off radial range on the lowest tilt ($\theta \approx 0.5°$) and a limited (80 km) cut-off radial range on the remaining tilts ($\theta \geq 1°$) for the reference check in the first step. As explained in section 2b, the cut-off radial ranges used in this paper are tuned and selected based on our extensive tests of the new method (as mentioned at the beginning of this section).

b. Squall-line case

As mentioned at the beginning of this section, the new method has been successfully tested with 12 900 volumes of radial velocity observations scanned by six operational radars in the central United States during the passage of a severe frontal squall-line storm system over the period of 9 days from 20 to 28 May 2005. An example is shown in Fig. 5a, which is the image of raw radial velocities scanned at $\theta = 1.3°$ by the operational KINX radar at 0838 UTC 23 May 2005 from the squall line. The spatial resolutions of the scans were 250 m in the radial direction and 1° in the azimuthal direction. At this time, the gust front of the squall line and associated wind shift zone were moving southeastward and just passed the radar site. Although the Nyquist velocity was as large as $v_N = 26.3$ m s^{-1}, the raw data were not free of alias. The strong northwesterly wind behind the gust front caused aliased velocities in the small red area marked by the white letter A in Fig. 5a.

Figure 5b shows that the aliased velocities in Fig. 5a are corrected by the new method without any false dealiasing. Note that the elevation angle is $\theta = 1.3°$ in this case, so the reference check goes from the smallest radial range up to $r = 80$ km (for $\theta \geq 1°$ as explained in section 2b). The aliased radial velocities in the small red area (marked by white letter A) in Fig. 5a are within this 80-km-range circle, and they are corrected mainly by the reference check in the first step, as revealed by the partially dealiased image produced at the end of the first step (not shown).

Figure 5c shows that the aliased velocities in Fig. 5a are also corrected by the operational method (Eilts and Smith 1990), but there are falsely dealiased radial velocities in the small bright-red area (marked by the white letter A in Fig. 5c) to the east of the radar within the 50-km-range circle. Note that these falsely dealiased radial velocities are distributed along an isolated narrow strip of scattered noisy data (as shown in Fig. 5a), and the false dealiasing appears to begin with a few bad seed data selected by the operational method from the scattered noisy raw data near the radar along each beam. As mentioned in the introduction, the operational method was designed to retain as much of the original data coverage as possible. Because of this, the dealiased radial velocities in Fig. 5c have essentially the same coverage as the raw data in Fig. 5a. As shown in Fig. 5a, there is a large isolated red area to the east of the radar outside the 150-km-range circle. This area is well retained by the operational method in Fig. 5c but is flagged by the new method and thus blackened in Fig. 5b. Clearly, this isolated area is beyond the 80-km range for the reference check, and the gap from this area to the main data

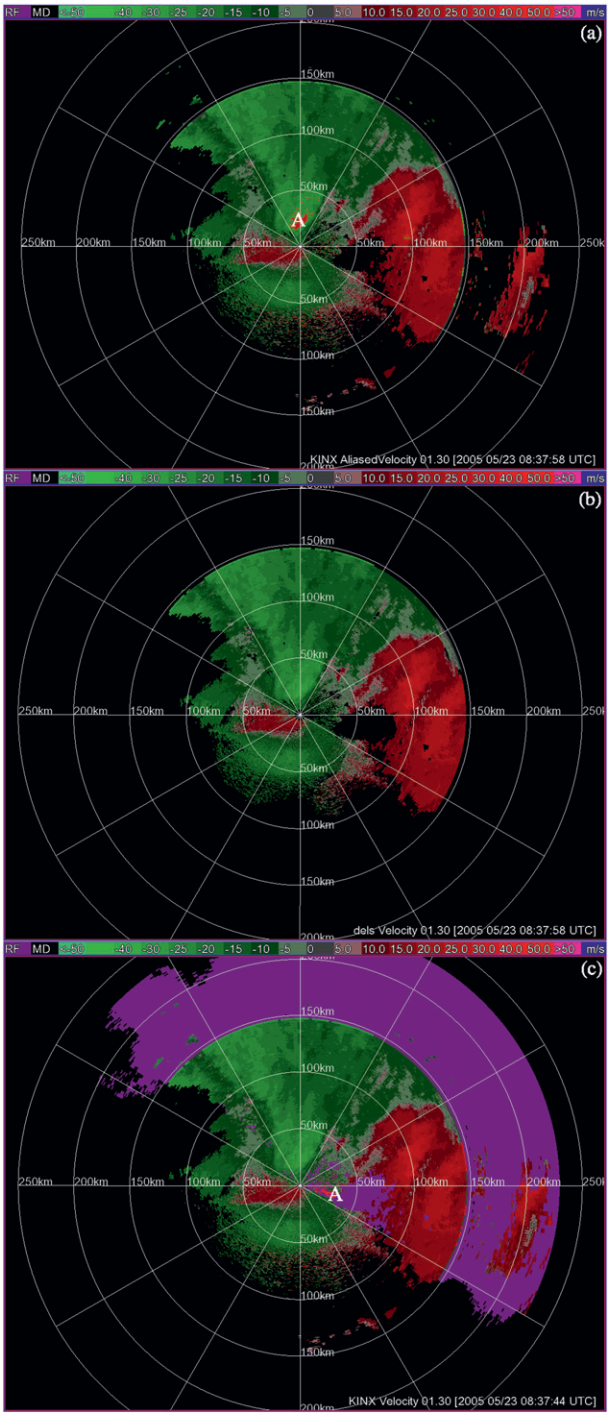

FIG. 5. (a) Raw level-II Doppler radial velocity image on 1.3° elevation from KINX radar at 0838 UTC 5 May 2005. (b) Dealiased radial velocity image by the new AR-VAD-based method. (c) Dealiased radial velocity image by the operational method. (a) The small red aliased velocity area is marked by the white letter A. (c) The small bright-red area of false dealiasing is marked by the white letter A. (c) The purple color shows data-void areas affected by range folding (RF), and (a),(b) these areas are blackened for clarity.

area (within a 150-km radial circle) is too large to pass through for the block-to-point continuity check in the new method.

c. *Cold-front case*

The new method has been also tested with real-time radial velocity observations from the KTLX radar and other operational WSR-88D radars under various weather conditions. An example is shown in Figs. 6a–c, which is a cold front case observed by the KTLX radar on 6 June 2008. Figure 6a is the image of raw radial velocities scanned at $\theta = 1.3°$ elevation from KTLX radar at 0309 UTC 6 June 2008. The spatial resolutions of the scans were 250 m in the radial direction and 1° in the azimuthal direction, while the Nyquist velocity was $v_N = 26.0$ m s^{-1}. At this time, the frontal rainband (oriented from southwest to northeast along and ahead of the cold front) was moving eastward and reached the radar site. The associated wind field was dominated by a strong southwesterly flow along the rainband in the lower troposphere. This strong northwesterly flow caused aliased velocities in the five red areas to the south and southwest of the radar and in the four green areas to the north of the radar (marked by the nine white letter As) in Fig. 6a.

Figure 6b shows that the aliased velocities in the five red areas to the south and southwest of the radar and in the nearest green area to the north of the radar in Fig. 6a are corrected by the new method without any false dealiasing. However, the remaining three green aliased velocity areas in Fig. 6a are flagged by the new method, and thus blackened in Fig. 6b. Note again that the elevation angle is $\theta = 1.3°$, so the reference check goes from the smallest radial range up to $r = 80$ km. The aliased radial velocities within this 80-km-range circle in Fig. 5a are well corrected by the reference check in the first step (not shown). The aliased radial velocities outside the 80-km range in the above-mentioned red areas and the nearest green area are largely corrected by the block-to-point continuity check. The remaining three green aliased velocity areas in Fig. 6a are beyond the 80-km range for the reference check. The two isolated green aliased velocity areas outside the 150-km-range circle are obviously too far to reach for the block-to-point continuity check. The green aliased velocity area between the 100- and 150-km-ange circles is close but not connected to the main data area (within the 100-km radial circle). The gap between this area and the main data area is narrow but partially filled with scattered noisy radial velocity data, so the block-to-point continuity check fails to pass through this gap.

Figure 6c shows that the operational method (Eilts and Smith 1990) is able to correct the aliased velocities in the five red areas and to correct most of the aliased

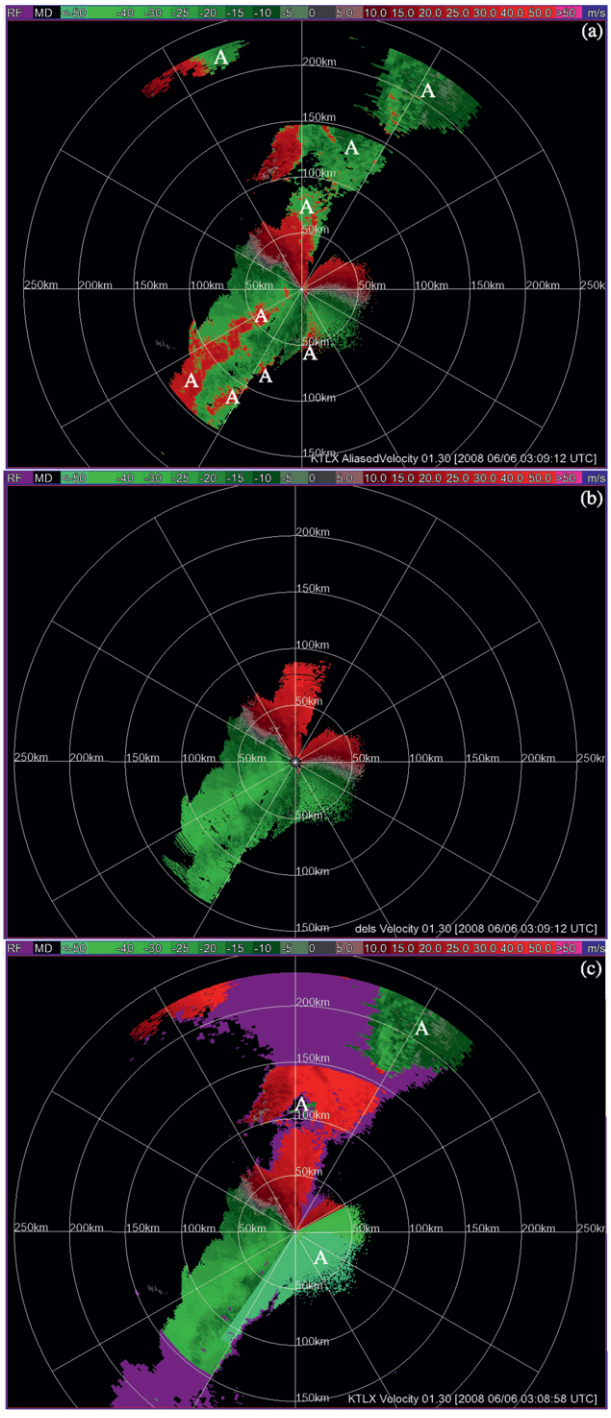

FIG. 6. (a) Raw level-II Doppler radial velocity image on 1.3° elevation from KTLX radar at 0309 UTC 6 Jun 2008. (b) Dealiased radial velocity image by the new AR-VAD-based method. (c) Dealiased radial velocity image by the operational method. (a) Nine aliased velocity areas are marked by the nine white letter "A"s. (c) Three areas of false dealiasing are marked by the three white letter "A"s. (c) The purple color shows data-void areas affected by RF, and (a),(b) these areas are blackened for clarity.

velocities in the three green areas to the north and northwest of the radar in Fig. 6a, but it fails to detect the aliased velocities in the green area to northeast of the radar outside the 150-km-range circle (marked by the white letter A in Fig. 6c). Additionally, and more seriously, the operational method produces falsely dealiased radial velocities over the entire 150° sector (marked by the white letter A in Fig. 6c) to the southeast of the radar. In this sector, the false dealiasing is apparently caused by bad seed data selected from the raw data nearest to the radar along each beam. Thus, the operational method is not ensured to be free of false dealiasing because it tends to retain as much of the original data coverage as possible.

d. High data quality standard required by radar data assimilation

Radial velocity observations from the operational WSR-88D have much higher spatial and temporal resolutions than the background resolutions provided by Weather Research and Forecasting (WRF) Nonhydrostatic Mesoscale Model (NMM) predictions for the regional data assimilation system at NCEP. Because of this, and because of the fact that the background errors are strongly correlated on the synoptic and mesoscale in the three- or four-dimensional space while radar observation errors are not correlated beyond neighboring gates or beams (Xu et al. 2007a,b), the WSR-88D observations can have significant resolution redundancy or information redundancy for the NCEP regional data assimilation system, or even a mesoscale data assimilation system (Xu 2007; Xu et al. 2009c). Redundant observations not only impose unnecessary computational burdens on a data assimilation system but can also cause the analysis to be ill conditioned. It is thus necessary to compress the observations into fewer superobservations (Purser et al. 2000; Liu et al. 2005b; Xu 2007). A simple way to do this is to average the data in the volume represented by each superobservation (Alpert and Kumar 2007). Because an alias or false dealiasing error is at least twice as large as the Nyquist velocity, and because the error it causes in the superobservation (through averaging) can be large but not tractable (after averaging) and can be difficult to detect, it is even more important to ensure that the data are free of alias or false dealiasing before the data are averaged into superobservations. This is the foremost important requirement for the new dealiasing method in this paper because it is developed primarily for radar data assimilation applications, while many previous dealiasing methods were developed primarily for visual and more limited quantitative applications, as mentioned in the introduction.

4. Discussion and conclusions

The new AR-VAD-based dealiasing method presented in this paper is a replacement of the previous Mod-VAD-based three-step dealiasing method in the radar data quality control package for radar data assimilation applications at NCEP (Liu et al. 2009). Eliminating or avoiding false dealiasing is the most important requirement for the method. To meet this requirement, not only is the Mod-VAD replaced by the AR-VAD, but the analysis is also restricted to not use any tilts below 1° (or 4°) for shallow (or deep) scans. In addition, the use of VAD wind for the reference check is restricted within a 30-km radial range on the lowest tilt ($\theta \approx 0.5°$) and within an 80-km radial range on the remaining tilts, and very stringent threshold conditions are used for alias corrections. With these major upgrades, the new method has been successfully tested with aliased radial velocity observations collected by operational WSR-88D radars for many different cases (as mentioned at the beginning of section 3).

The new method has been also tested with real-time radial velocity observations from the KTLX radar and other operational WSR-88D radars under various weather conditions. The real-time tests show that the method is capable of correcting most alias errors without false dealiasing (see the example in Fig. 6), but it tends to reject too many data around and above strongly sheared inversion layers for severe winter ice storms scanned by the VCP31 mode with the Nyquist velocity reduced below 12 m s^{-1} (not shown in this paper). In the latter case (VCP31), the estimated VAD wind often cannot pass the stringent vertical continuity check [see (1)], so the vertical profile of the VAD wind is severely limited below the inversion layer. Additionally, the AR-VAD analysis is inherently limited by the VAD uniform-wind approximation, so the VAD-produced reference radial velocities do not have the required variability that allows most data to pass those stringent threshold conditions in the reference check [see (4)–(5)], which are further narrowed by the reduced Nyquist velocity.

The VAD uniform-wind approximation becomes poor or even invalid for either intense rotational winds in a mesocyclone or hurricane core area, or for highly nonuniform winds in the vicinity of a sharp front. When a mesocyclone or hurricane core moves into the radial range covered by the VAD-based reference check, the reference check tends to flag too many data in the mesocyclone or the hurricane core in the first step and makes the block-to-point continuity check hard to correct or deflag, even though the Nyquist velocity is not small in this case. This is an obvious limitation of the new, or any, VAD-based method. In particular, when the wind field is highly nonuniform (in association with a sharp front that just passes through the radar site) and the AR-VAD fails to produce a reference wind profile in the first step, then the new AR-VAD-based method fails to perform. In addition, the new method requires adequate data coverage to perform the AR-VAD analysis, and it tends to reject isolated data areas far away from the radar when these areas are beyond the reach of reference check and subsequent continuity check (as seen from the examples in Figs. 5 and 6). This is another limitation of the new method.

The problem with VCP31 scans has been also a difficult challenge for the operationally used dealiasing technique at NWS Radar Operations Center (Burgess and Crum 2009; Witt et al. 2009). Good progress and initial success has been made in solving the problem with VCP31 scans by using the alias-robust variational analysis (Xu et al. 2009a, section 3.2) in place of the AR-VAD analysis for the reference check (Xu et al. 2009b, section 4). This success will serve as a paradigm for solving other above-mentioned limitations of the new method. In particular, the alias-robust variational analysis can be further extended and applied adaptively to various isolated data areas, even with reduced Nyquist velocities. This approach will be explored to make the method more powerful and adaptive to deal with each type of difficult scenarios for not only the NWS WSR-88D radars, but also Federal Aviation Administration (FAA) airport Terminal Doppler Weather Radars (with the Nyquist velocity reduced to about 15 m s^{-1}). Continued effort is undertaken in this direction to further improve the dealiasing technique in the data quality control package dedicated for radar data assimilation applications at NCEP.

Acknowledgments. The authors are thankful to Don Burgess, Dusan Zrnić, and anonymous reviewers for their comments and suggestions that improved the presentation of the results, and to Xiaobin Qiu for his help in producing the flowcharts in Figs. 1–3. The research work was supported by the NOAA HPCC program, the NCEP–NSSL collaborative project on radar data quality control, and ONR Grants N000140410312 and N000141010778 to the University of Oklahoma. Funding was also provided by NOAA/Office of Oceanic and Atmospheric Research under the NOAA–University of Oklahoma Cooperative Agreement NA17RJ1227, U.S. Department of Commerce.

REFERENCES

Alpert, J. C., and V. K. Kumar, 2007: Radial wind super-obs from the WSR-88D radars in the NCEP operational assimilation system. *Mon. Wea. Rev.,* **135,** 1090–1109.

Bergen, D. W., and R. C. Brown, 1980: Interactive radar velocity unfolding. Preprints, *19th Conf. on Radar Meteorology,* Miami, FL, Amer. Meteor. Soc., 278–283.

Bergen, W. R., and S. C. Albers, 1988: Two- and three-dimensional de-aliasing of Doppler radar velocities. *J. Atmos. Oceanic Technol.,* **5,** 305–319.

Browning, K. A., and R. Wexler, 1968: The determination of kinematic properties of a wind field using Doppler radar. *J. Appl. Meteor.,* **7,** 105–113.

Burgess, D. W., and T. Crum, 2009: Observed failure modes of the WSR-88D velocity dealiasing algorithm during severe weather outbreaks. Preprints, *34rd Conf. on Radar Meteorology,* Williamsburg, VA, Amer. Meteor. Soc., P5.16. [Available online at http://ams.confex.com/ams/pdfpapers/156056.pdf.]

Doviak, J. D., and D. S. Zrnić, 2006: *Doppler Radar and Weather Observations*. 2nd ed. Dover Publications, 562 pp.

Eilts, M. D., and S. D. Smith, 1990: Efficient dealiasing of Doppler velocities using local environment constraints. *J. Atmos. Oceanic Technol.,* **7,** 118–128.

Frush, C., R. J. Doviak, M. Sachidananda, and D. S. Zrnić, 2002: Application of the SZ phase code to mitigate range–velocity ambiguities in weather radars. *J. Atmos. Oceanic Technol.,* **19,** 413–430.

Gao, J., K. K. Droegemeier, J. Gong, and Q. Xu, 2004: A method for retrieving mean horizontal wind profiles from single-Doppler radar observations contaminated by aliasing. *Mon. Wea. Rev.,* **132,** 1399–1409.

Gong, J., L. Wang, and Q. Xu, 2003: A three-step dealiasing method for Doppler velocity data quality control. *J. Atmos. Oceanic Technol.,* **20,** 1738–1748.

Haase, G., and T. Landelius, 2004: Dealiasing of Doppler radar velocities using a torus mapping. *J. Atmos. Oceanic Technol.,* **21,** 1566–1573.

Hennington, L., 1981: Reducing the effects of Doppler radar ambiguities. *J. Appl. Meteor.,* **20,** 1543–1546.

James, C. N., and R. A. Houze, 2001: A real-time four-dimensional Doppler dealiasing scheme. *J. Atmos. Oceanic Technol.,* **18,** 1674–1683.

Jing, Z., and G. Wiener, 1993: Two-dimensional dealiasing of Doppler velocities. *J. Atmos. Oceanic Technol.,* **10,** 798–808.

Lhermitte, R. M., and D. Atlas, 1961: Precipitation motion by pulse Doppler. Preprints, *Ninth Weather Radar Conf.,* Kansas City, MO, Amer. Meteor. Soc., 218–223.

Liu, S., Q. Xu, and P. Zhang, 2005a: Quality control of Doppler velocities contaminated by migrating birds. Part II: Bayes identification and probability tests. *J. Atmos. Oceanic Technol.,* **22,** 1114–1121.

——, M. Xue, J. Gao, and D. Parrish, 2005b: Analysis and impact of super-obbed Doppler radial velocity in the NCEP grid-point statistical interpolation (GSI) analysis system. *Extended Abstracts, 17th Conf. Numerical Weather Prediction,* Washington, DC, Amer. Meteor. Soc., 13A.4.

——, and Coauthors, 2009: WSR-88D radar data processing at NCEP. Preprints, *34th Conf. on Radar Meteorology,* Williamsburg, VA, Amer. Meteor. Soc., 14.2. [Available online at http://ams.confex.com/ams/pdfpapers/156011.pdf.]

Purser, R. J., D. F. Parrish, and M. Masutani, 2000: Meteorological observational data compression; An alternative to conventional ''super-Obbing.'' National Centers for Environmental Prediction Office Note 430, 12 pp.

Ray, P., and C. Ziegler, 1977: Dealiasing first moment Doppler estimates. *J. Appl. Meteor.,* **16,** 563–564.

Tabary, P., G. Scialom, and U. Germann, 2001: Real-time retrieval of the wind from aliased velocities measured by Doppler radars. *J. Atmos. Oceanic Technol.,* **18,** 875–882.

Torres, S. M., Y. F. Dubel, and D. S. Zrnic, 2004: Design, implementation, and demonstration of a staggered PRT algorithm for the WSR-88D. *J. Atmos. Oceanic Technol.,* **21,** 1389–1399.

Witt, A., R. A. Brown, and Z. Jing, 2009: Performance of a new velocity dealiasing algorithm for the WSR-88D. Preprints, *34rd Conf. on Radar Meteorology,* Williamsburg, VA, Amer. Meteor. Soc., P4.8. [Available online at http://ams.confex.com/ams/pdfpapers/155951.pdf.]

Xu, Q., 2007: Measuring information content from observations for data assimilation: Relative entropy versus Shannon entropy difference. *Tellus,* **59A,** 198–209.

——, K. Nai, and L. Wei, 2007a: An innovation method for estimating radar radial-velocity observation error and background wind error covariances. *Quart. J. Roy. Meteor. Soc.,* **133,** 407–415.

——, ——, ——, H. Lu, P. Zhang, S. Liu, and D. Parrish, 2007b: Estimating radar wind observation error and NCEP WRF background wind error covariances from radar radial-velocity innovations. Preprints, *18th Conf. on Numerical Weather Prediction,* Park City, UT, Amer. Meteor. Soc., 1B.3. [Available online at http://ams.confex.com/ams/pdfpapers/123419.pdf.]

——, ——, ——, and Q. Zhao, 2009a: An unconventional approach for assimilating aliased radar radial velocities. *Tellus,* **61A,** 621–630.

——, ——, P. Zhang, S. Liu, and D. Parrish, 2009b: A new dealiasing method for Doppler velocity data quality control. Preprints, *34th Conf. on Radar Meteorology,* Williamsburg, VA, Amer. Meteor. Soc., P9.6. [Available online at http://ams.confex.com/ams/pdfpapers/155947.pdf.]

——, L. Wei, and S. Healy, 2009c: Measuring information content from observations for data assimilations: Connection between different measures and application to radar scan design. *Tellus,* **61A,** 144–153.

——, K. Nai, and L. Wei, 2010: Fitting VAD wind to aliased radial-velocity observations—A minimization problem with multiple minima. *Quart. J. Roy. Meteor. Soc.,* **136,** 451–461.

Yamada, Y., and M. Chong, 1999: VAD-based determination of the Nyquist interval number of Doppler velocity aliasing without wind information. *J. Meteor. Soc. Japan,* **77,** 447–457.

Zhang, J., and S. Wang, 2006: An automated 2D multipass Doppler radar volocity dealiasing scheme. *J. Atmos. Oceanic Technol.,* **23,** 1239–1248.

Zhang, P., S. Liu, and Q. Xu, 2005: Quality control of Doppler velocities contaminated by migrating birds. Part I: Feature extraction and quality control parameters. *J. Atmos. Oceanic Technol.,* **22,** 1105–1113.

Zhu, L., and J. Gong, 2006: A study on application OIQC method to velocity dealiasing of Doppler radar VAD velocity data. *Plateau Meteorology,* **25,** 862–869.